

Inferring the parameters of a Markov process from snapshots of the steady state

Simon L. Dettmer and Johannes Berg*

Institute for Theoretical Physics, University of Cologne, Zùlpicher StraÙe 77, 50937 Cologne, Germany

We seek to infer the parameters of an ergodic Markov process from samples taken independently from the steady state. Our focus is on non-equilibrium processes, where the steady state is not described by the Boltzmann measure, but is generally unknown and hard to compute. To this end, we propose a quantity we call propagator likelihood, which takes on the role of the likelihood in equilibrium processes. This propagator likelihood is based on fictitious transitions between those configurations of the system which occur in the samples. The propagator likelihood can be derived by minimising the relative entropy between the empirical distribution and a distribution generated by propagating the empirical distribution forward in time. Maximising this propagator likelihood leads to an efficient reconstruction of the parameters of the underlying model in different systems, both with discrete configurations and with continuous configurations. We apply the method to different non-equilibrium models from statistical physics and theoretical biology, including the asymmetric simple exclusion process (ASEP), the kinetic Ising model, and replicator dynamics.

PACS numbers: 02.50.Ga,02.30.Zz,02.50.Tt,89.75.-k 75.50.Lk,05.70.Ln

Keywords: stochastic inference, Markov process, non-equilibrium steady state, Ising model, neural networks, replicator dynamics, asymmetric exclusion process, disordered systems

INTRODUCTION

The problem of inferring the parameters of a stochastic model from data is ubiquitous in the natural and social sciences, and engineering. Many systems, like gene regulatory networks, electric power grids, virus populations, or financial markets have a complex dynamics which is often modelled by stochastic processes. Such stochastic processes are characterised by potentially many free parameters, which need to be estimated from data. For a review in the context of the inverse Ising problem, see [1]. Here, we ask how to infer the parameters characterising a non-equilibrium stochastic process.

An important class of stochastic processes is Markov processes, which are fully defined by instantaneous transition rates. For a Markov process, the future dynamics of the system depends on the history of the process only via its present configuration. We consider a system with configurations x in some configuration space with time-homogeneous transition probabilities between configurations. Configurations can be discrete or continuous, and also time can be discrete or continuous. For the concrete example of a colloidal particle undergoing Brownian motion, the configurations x are positions in space and the model parameter specifies the diffusion constant of the particle. We restrict ourselves to ergodic processes, so for any initial state the system eventually settles into a unique steady state characterised by the steady-state probability distribution $p_{\Theta}(x)$. Our aim is to infer the underlying parameters Θ^{true} from M samples x^{μ} , with $\mu = 1, \dots, M$, drawn independently from the steady state distribution.

In general, the inference of parameters hinges on the description of the empirical data by the model. For a model whose steady state $p_{\Theta}(x)$ is known explicitly, the

maximum-likelihood estimate

$$\Theta^{\text{inf}} = \underset{\Theta}{\operatorname{argmax}} \prod_{\mu=1}^M p_{\Theta}(x^{\mu}) \quad (1)$$

provides an estimate of the model parameters which becomes exact in the limit of a large number of samples. However, for non-equilibrium models, the steady state is hard to compute. In some cases, time series data is available. In such cases, one can use the empirically observed transitions between configurations to compute the likelihood of the observed trajectories. This likelihood can be computed directly from the transition probabilities specified by the model; the underlying model parameters are then estimated as the parameters that maximise the likelihood of the time series [2, 3]. Inference from time series can be performed even more efficiently by applying mean-field approximations [2, 4, 5].

However, for many systems, classical as well as quantum, time series data is not available. An extreme case is whole-genome single-cell gene expression profiling, where cells are destroyed by the measurement process. In such cases, we have only independent samples as data from which to infer the model parameters. To this end, we use the transition rates between configurations and their dependence on the model parameters to construct a quantity we call the propagator likelihood and show how this likelihood can be used to infer the model parameters from independent samples taken from the steady state.

This article is organised as follows: First, we introduce the propagator likelihood through an intuitive argument and then offer a systematic derivation based on a relative-entropy argument. Second, we apply the propagator likelihood to pedagogical examples with both discrete and continuous configurations, specifically the asymmetric simple exclusion process (ASEP) and the Ornstein-

Uhlenbeck process. Finally, we address the more challenging problem of inferring the parameters of two prominent models from statistical physics and theoretical biology: the kinetic Ising model and replicator dynamics.

THE PROPAGATOR LIKELIHOOD

Suppose we knew the functional dependence of the steady-state distribution $p_{\Theta}(x)$ on the model parameters Θ . Then a standard approach would be to maximise the (log-) likelihood of the samples,

$$\mathcal{L}(\Theta) = \frac{1}{M} \sum_{\mu=1}^M \log p_{\Theta}(x^{\mu}) = \sum_x \hat{p}(x) \log p_{\Theta}(x), \quad (2)$$

where the set of sampled configurations characterises the empirical distribution $\hat{p}(x)$ with probability mass function

$$\hat{p}(x) = \frac{1}{M} \sum_{\mu=1}^M \delta_{x^{\mu}, x}. \quad (3)$$

$\delta_{x^{\mu}, x}$ denotes a Kronecker- δ .

However, in non-equilibrium systems we frequently do not know the steady-state distribution. Non-equilibrium systems lack detailed balance, so the steady state is not described by the Boltzmann distribution, and lacks a simple characterisation. Our solution to this inference problem in such cases is based on exploiting one elementary fact: since the distribution p_{Θ} is stationary, it remains unchanged if we propagate forward in time by an arbitrary time τ . Thus, we can replace the steady-state distribution $p_{\Theta}(x)$ in the log-likelihood function (2) with a version propagated in time, $\sum_y p_{\Theta}(x, \tau|y, 0)p_{\Theta}(y)$. The propagator $p_{\Theta}(x, \tau|y, 0)$ is the conditional probability of observing the system in configuration x at time $t = \tau$, given it was in configuration y at time $t = 0$. By further replacing the unknown steady-state distribution $p_{\Theta}(y)$ with the empirical distribution $\hat{p}(y)$, we arrive at the propagator likelihood

$$\begin{aligned} \mathcal{P}\mathcal{L}(\Theta; \tau) &= \sum_x \hat{p}(x) \log \sum_y p_{\Theta}(x, \tau|y, 0) \hat{p}(y) \\ &= \frac{1}{M} \sum_{\mu=1}^M \log \left(\frac{1}{M} \sum_{\nu=1}^M p_{\Theta}(x^{\mu}, \tau|x^{\nu}, 0) \right). \end{aligned} \quad (4)$$

In this way, we have moved the parameter-dependence from the (unknown) steady-state distribution $p_{\Theta}(x)$ to the (known) propagator $p_{\Theta}(x, \tau|y, 0)$. Although using only configurations sampled independently with no sense of temporal order, the propagator likelihood effectively considers fictitious transitions $x^{\nu} \xrightarrow{\tau} x^{\mu}$ between all pairs of sampled configurations. For models with continuous configurations, $p_{\Theta}(x^{\mu}, \tau|x^{\nu}, 0)$ is the transition probability density.

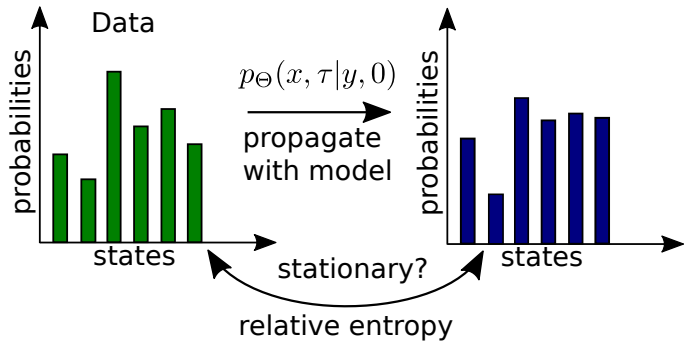


FIG. 1. The propagator likelihood. The independent samples $\{x^{\mu}\}_{\mu=1}^M$ define the empirical distribution \hat{p} defined by equation (3), shown on the left. We fix an arbitrary time τ and use the known transition probabilities $p_{\Theta}(x, \tau|y, 0)$ to propagate \hat{p} in time and generate a new distribution $q_{\Theta, \tau}$ (see Eq.(5)), shown on the right. Demanding stationarity of the model, we can estimate the underlying parameters Θ^{true} by finding the parameters Θ^{inf} that minimise the distance between \hat{p} and $q_{\Theta, \tau}$ as measured with relative entropy. This is equivalent to maximising the propagator likelihood (see main text).

Minimising relative entropy

We rephrase the inference problem as finding a set of parameters Θ such that the propagator $p_{\Theta}(x, \tau|y, 0)$ is compatible with the empirical distribution \hat{p} being stationary (see Fig. 1). Demanding stationarity corresponds to requiring that \hat{p} is in some sense close to a distribution $q_{\Theta, \tau}$ generated by propagating the empirical distribution for an arbitrary time τ ,

$$q_{\Theta, \tau}(x) = \sum_y p_{\Theta}(x, \tau|y, 0) \hat{p}(y). \quad (5)$$

To quantify this notion of closeness for discrete configurations, we use the relative entropy or Kullback-Leibler divergence [6]

$$D(\hat{p}||q_{\Theta, \tau}) = \sum_x \hat{p}(x) \log \frac{\hat{p}(x)}{q_{\Theta, \tau}(x)}. \quad (6)$$

Inserting the probability mass function $q_{\Theta, \tau}(x)$ defined by (5) into the relative entropy, we find that the relative entropy can be written as the negative sum of the Shannon entropy of the empirical distribution, $S(\hat{p}) = -\sum_x \hat{p}(x) \log \hat{p}(x)$ and the propagator likelihood (4):

$$D(\hat{p}||q_{\Theta, \tau}) = -S(\hat{p}) - \mathcal{P}\mathcal{L}(\Theta; \tau). \quad (7)$$

The first term depends only on the sampled configurations and is independent of the model parameters; thus minimising the relative entropy over Θ is equivalent to maximising the propagator likelihood. Furthermore, due to the positivity of relative entropy, the propagator likelihood is bounded from above by the negative Shannon

entropy, and this bound will be saturated only for a perfectly stationary model.

For models with continuous configurations, the relative entropy (6) cannot be defined, since the propagated distribution $q_{\Theta,\tau}(x)$ is continuous, while the empirical distribution $\hat{p}(x)$ is discrete. However, the propagator likelihood (4) is well-defined for both discrete and continuous state spaces.

For long propagation times τ , the propagator likelihood converges to the standard log-likelihood (2), since $\lim_{\tau \rightarrow \infty} q_{\Theta,\tau}(x) \equiv p_{\Theta}(x)$ for ergodic systems. However, in general the complexity of calculating the propagator increases with τ . For models with discrete time, the single-step propagator takes the form of a (usually high-dimensional) matrix, from which propagators for longer times can in principle be computed by taking powers of this matrix.

MODELS WITH DISCRETE CONFIGURATIONS

Discrete time: a simple two-configuration model

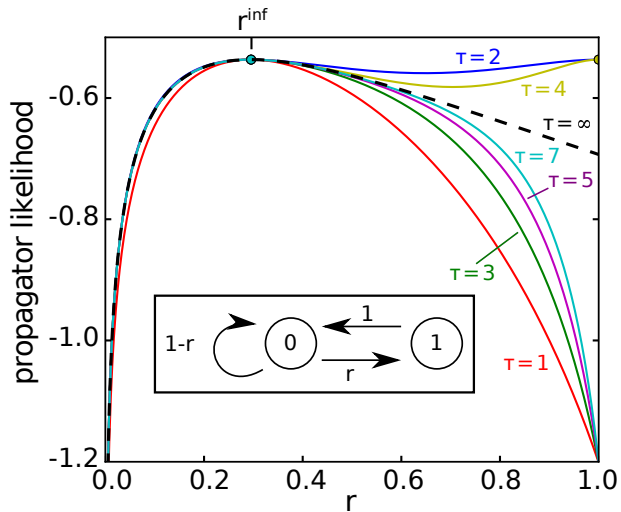


FIG. 2. The propagator likelihood for a simple two-configuration system. The inset shows the single-step dynamics of the system with configurations 0 and 1, controlled by the hopping probability $r \in (0, 1)$. In the main figure, the solid lines show the propagator likelihood for varying propagation times τ . The dashed line shows the log-likelihood (2), which corresponds to an infinite propagation time. The maximum likelihood estimate of the hopping probability, $r^{\text{inf}} = \frac{1-\hat{p}(0)}{\hat{p}(0)}$, is marked on the top axis and coincides with the maximum for all propagator likelihoods with an uneven number of time steps τ (see the main text for an explanation of even numbers of time steps).

To illustrate the propagator likelihood with a toy example, we consider a system with only two configurations, denoted by 0 and 1 (see inset of Fig. 2). At each

time step, if the system is in configuration 1, it moves to configuration 0. If it is in configuration 0, it moves to configuration 1 with probability $r \in (0, 1)$ or remains in configuration 0 with probability $1 - r$. In this simple model, the steady-state distribution is easily computed, giving $p_r(0) = 1/(1+r)$ and $p_r(1) = 1 - p_r(0) = r/(1+r)$.

We are now given samples $\{x^\mu\}_{\mu=1}^M \in \{0, 1\}^M$ taken independently from the steady state and want to infer the model parameter r . The empirical distribution is given by the frequencies of the two configurations, $\hat{p}(0) = \frac{1}{M} \sum_{\mu=1}^M \delta_{0,x^\mu}$ and $\hat{p}(1) = 1 - \hat{p}(0)$. In this case, since we know the steady state, we can infer r from the relationship $\langle \hat{p}(0) \rangle = 1/(1+r)$, yielding $r^{\text{inf}} = (1 - \hat{p}(0))/\hat{p}(0)$. For comparison, we also use the propagator likelihood (4) with the single-step propagator $p_r(x, \tau = 1 | y, 0) = \delta_{y,1} \delta_{x,0} + \delta_{y,0} (r \delta_{x,1} + (1-r) \delta_{x,0})$, giving

$$\begin{aligned} \mathcal{PL}(r; 1) &= \hat{p}_0 \log \left(\underbrace{(1-r)\hat{p}_0}_{0 \rightarrow 0} + \underbrace{\hat{p}_1}_{1 \rightarrow 0} \right) + \hat{p}_1 \log \left(\underbrace{r\hat{p}_0}_{0 \rightarrow 1} \right) \\ &= \hat{p}_0 \log(1 - r\hat{p}_0) + (1 - \hat{p}_0) \log(r\hat{p}_0). \end{aligned} \quad (8)$$

Maximising this propagator likelihood analytically with respect to r , by setting $\frac{d\mathcal{PL}}{dr}(r^{\text{inf}}) = 0$, we recover the same result as obtained above from analysing the known steady-state distribution. Indeed, for uneven propagation times, the propagator likelihood shows a unique maximum at the correct value $r^{\text{inf}} = \frac{1-\hat{p}_0}{\hat{p}_0}$ and approaches the log-likelihood for increasing τ , as expected (see Fig. 2). For even propagation times, however, a second (global) maximum occurs at the boundary $r = 1$: since the choice $r = 1$ makes the two configurations simply exchange their probabilities in each step, any distribution becomes stationary over an even number of time steps and the system loses its ergodicity. Canonically, we use the single-step propagator for inferring system parameters in models with discrete time; therefore such periodicity issues cannot arise.

Continuous time: the asymmetric simple exclusion process (ASEP)

As an example of a model with continuous time, we consider the asymmetric simple exclusion process (ASEP) on a ring with asynchronous updates (see inset of Fig. 3). The ASEP is a simple model of a driven lattice gas and has been applied to traffic flow, surface growth, and directed paths in random media [7–9].

The steady-state distribution in 1D can be calculated analytically in terms of matrix products [8, 9]. In higher dimensions, however, there is no such systematic approach and, to the best of our knowledge, the steady-state distribution is unknown.

The model consists of K particles moving on a periodic one-dimensional lattice with $N > K$ lattice sites.

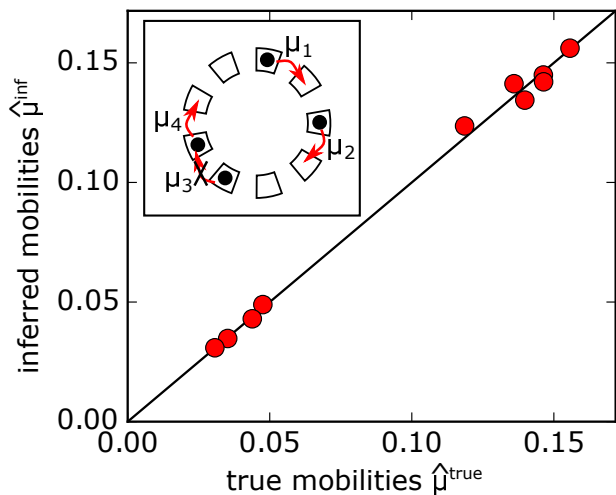


FIG. 3. Reconstruction of hopping rates in the asymmetric simple exclusion process (ASEP). The inset schematically shows the dynamics: K particles move on a periodic one-dimensional lattice with $N > K$ lattice sites, see text. In the main figure, we plot the relative mobilities $\hat{\mu}_i^{\text{inf}}$ inferred using the propagator likelihood versus the underlying relative mobilities $\hat{\mu}_i^{\text{true}} = \mu_i^{\text{true}} / \sum_j \mu_j^{\text{true}}$ that were used to generate the data. We simulated $K = 10$ particles hopping on a lattice with $N = 15$ sites and took $M = 10^{10}$ samples independently from the steady state. The underlying mobilities μ_i were drawn independently from a uniform distribution on the unit interval $(0, 1)$.

Each lattice site can be occupied by at most one particle. Particles labelled $i = 1, \dots, K$ independently attempt to jump one step in the clockwise direction at a rate μ_i called their intrinsic mobility or hopping rate. Transitions between different configurations occur at discrete random times T_1, T_2, \dots , and the waiting time between the jumps is exponentially distributed with parameter $\mu_1 + \mu_2 + \dots + \mu_K$.

The configuration of the system can be characterised by the number of free lattice sites in front of each particle, $\mathbf{n} = (n_1, \dots, n_K) \subset (\mathbb{N}_0)^K$, with the restriction that all lattice sites are occupied: $n_1 + n_2 + \dots + n_K = N - K$. The easiest way of stating the propagator is in terms of the numbers of such free lattice sites.

Since the steady-state distribution $p_\mu(\mathbf{n})$ itself is not associated with a time scale, we need to eliminate one parameter by rescaling time. We choose to measure time in units such that $\mu_1 + \mu_2 + \dots + \mu_K = 1$. The steady-state distribution is then determined only by the relative hopping rates $\hat{\mu}_i := \mu_i / \sum_j \mu_j$. In the propagator likelihood we consider the distribution of the next configuration \mathbf{n}' that is visited by the process after starting in configuration \mathbf{n} . The transition probabilities are then determined by the relative hopping rates $\hat{\mu}_i$. Alternatively, in the general framework of propagators, we choose as the propagation time the (random) instant of the first jump, $\tau = T_1$, when a (random) particle I attempts to move one

step in the clockwise direction. This random variable T_1 varies jointly with the configurations $\mathbf{n}(t)$ over different realisations of the process and its marginal distribution is irrelevant. Choosing $\tau = T_1$ simply corresponds to conditioning on the event that exactly one (attempted) jump has taken place. The single-step propagator is then defined as the probability that this first jump leads to a transition from configuration $\mathbf{n} = (n_1, \dots, n_K)$ to a new configuration $\mathbf{n}' = (n'_1, \dots, n'_K)$.

We use the law of total probability to decompose the propagator into the contributions from different particles that may attempt a jump at T_1 , giving

$$p_{\hat{\mu}}(\mathbf{n}', T_1 | \mathbf{n}, 0) = \sum_{i=1}^K p_{\hat{\mu}}(\mathbf{n}', T_1 | \mathbf{n}, 0, I = i) P(I = i). \quad (9)$$

The probability that a specific particle i attempts to jump is equal to its relative hopping rate

$$P(I = i) = \left(\frac{\mu_i}{\sum_{j=1}^K \mu_j} \right). \quad (10)$$

Given that particle i attempts to jump, two things can happen: if the place in front of particle i is already occupied ($n_i = 0$), the jump is unsuccessful and the system remains in the same configuration, $\mathbf{n}' = \mathbf{n}$. Otherwise, the jump is successful and particle i hops one place forward to a free lattice site, decreasing the gap in front of it by one, $n_i \rightarrow n_i - 1$, and increasing the gap behind it by one, $n_{i-1} \rightarrow n_{i-1} + 1$ (we define $n_0 \equiv n_K$ due to the periodic boundary condition). All other gaps remain unaffected. The resulting propagator is

$$p_{\hat{\mu}}(\mathbf{n}', T_1 | \mathbf{n}, 0, I = i) = \delta_{n_i, 0} \prod_j \delta_{n'_j, n_j} + \delta_{n'_i, n_i - 1} \delta_{n'_{i-1}, n_{i-1} + 1} \prod_{j \neq i, i-1} \delta_{n'_j, n_j}. \quad (11)$$

We use this result to evaluate the propagator likelihood (4) and infer the relative mobilities $\hat{\mu}_i$ of $K = 10$ particles hopping on $N = 15$ lattice sites. The particle mobilities μ_i are drawn uniformly from the interval $(0, 1)$. We generate $M = 10^{10}$ Monte Carlo samples, recorded every 10 jumps after an initial settling time of 10^5 jumps to reach the steady state. We then maximise the propagator likelihood numerically with the sequential least squares programming algorithm, as implemented in the SciPy library [10]. In Fig. 3 we plot the inferred relative mobilities versus the relative mobilities used to generate the samples.

MODELS WITH CONTINUOUS CONFIGURATIONS

Markov processes with continuous configurations pose an additional challenge: Finite-time propagators are gen-

erally not known explicitly. Instead, they are characterised indirectly as the solution of a Fokker-Planck equation. Rather than solving a Fokker-Planck equation, which for systems with a large number of degrees of freedom is generally infeasible, we proceed by approximating the propagator for short times τ via a linearisation of the corresponding Langevin equation (LE) that describes the stochastic dynamics of the model.

Again, we illustrate this procedure for a toy model. We consider one of the simplest processes with continuous configurations, the Ornstein-Uhlenbeck process (OUP), which describes the Brownian dynamics of an overdamped particle in a quadratic potential. Note that, again, for this particular case the steady-state distribution is known exactly, so we could infer the model parameters using the standard maximum likelihood approach. Nonetheless, we infer the parameters of the OUP using the propagator likelihood before turning to more complex models where the likelihood-based approach is not feasible.

The Ornstein-Uhlenbeck process

We consider a single particle diffusing in a one-dimensional harmonic potential $U(x) = \frac{b}{2}x^2$ with diffusion constant σ^2 . A physical realisation of this model is a colloidal particle in solution being held in place by optical tweezers and confined to a one-dimensional channel. The dynamics of the particle is modelled by the Langevin equation

$$\frac{dx}{dt} = -bx + \sigma\xi(t), \quad (12)$$

where the random force $\xi(t)$ is described by δ -correlated white noise interpreted in the Itô convention.

As for the exclusion process, we must eliminate one parameter by rescaling time, since the steady-state distribution is time-independent. We consider the dimensionless time $t' = t\sigma^2$ such that the particle has unit diffusivity. To calculate the propagator likelihood for short times $\tau \ll 1$, we linearise the LE (12) in time

$$x(\tau) \approx x(0) - \frac{b}{\sigma^2}x(0)\tau + \int_0^\tau dt' \xi(t'). \quad (13)$$

Since the integrated white noise $\int_0^\tau dt' \xi(t')$ is normally distributed with mean 0 and variance τ , we obtain the approximate Gaussian propagator

$$p_{b/\sigma^2}(x, \tau|y, 0) \approx \frac{\exp(-[x - \bar{x}]^2/2\tau)}{\sqrt{2\pi\tau}}, \quad (14)$$

where $\bar{x} = y - (b/\sigma^2)y\tau$ is the most likely future position of the particle.

Such a Gaussian form of the propagator emerges for any linearised LE with white noise and is not specific

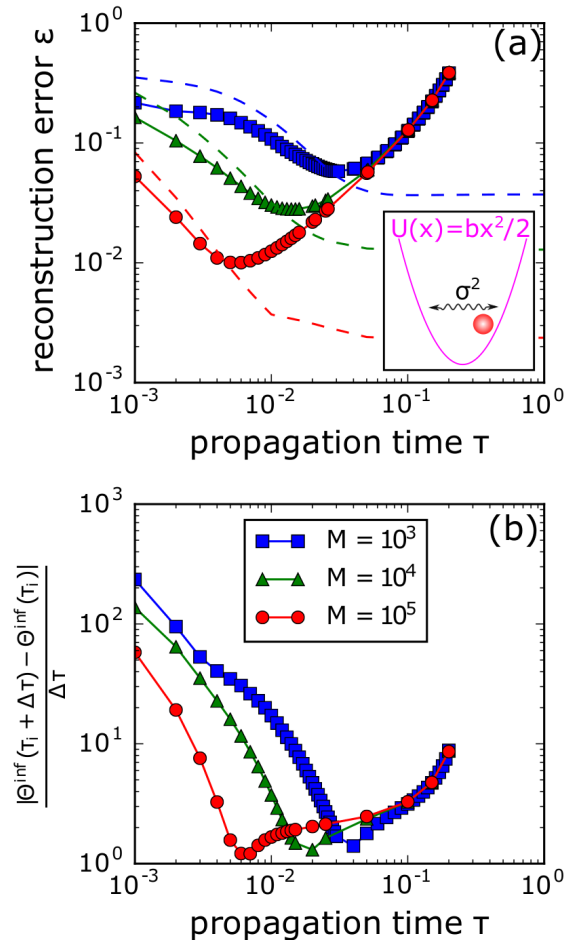


FIG. 4. Parameter inference in the Ornstein-Uhlenbeck process. (a) The inset shows a schematic plot of the model describing a single particle moving in the harmonic potential $U(x) = bx^2/2$. In the main figure, we show the relative reconstruction error $\epsilon = |\Theta^{\text{inf}} - \Theta^{\text{true}}|/\Theta^{\text{true}}$ of the parameter $\Theta = b/\sigma^2$ (characterising the steady state) versus the dimensionless propagation time τ used in the propagator for sample sizes $M = 10^3$ (\blacksquare), $M = 10^4$ (\blacktriangle), and $M = 10^5$ (\bullet). The solid lines with markers show the reconstruction errors for the approximate short-time propagator, the dashed lines indicate the reconstruction errors for the exact finite-time propagator. (b) shows the estimated rate of change of the inferred parameter with respect to the propagation time used as computed with the forward difference quotients: $|\partial\Theta^{\text{inf}}/\partial\tau(\tau_i)| \approx |\Theta^{\text{inf}}(\tau_i + \Delta\tau) - \Theta^{\text{inf}}(\tau_i)|/\Delta\tau$, shown on the vertical axis for the differentiation step size $\Delta\tau = 10^{-3}$. The minimal rate of change corresponds to the optimal choice of the propagation time (see main text).

The data was generated by independent sampling from the stationary distribution, i.e. a centred Gaussian with variance $\sigma^2/(2b) = 1/4$. In order to remove fluctuations between different sample sets $\{x_\mu\}_{\mu=1}^M$ and demonstrate the dependence of the average error on the sample size M and propagation time τ , the results were averaged over 50 independent sample sets. The equivalence of the minima of the reconstruction error and the rate of change hold true on the level of individual sample sets, while the position of the minima may vary between different sample sets.

to the OUP. For coloured, multiplicative noise, $\xi(t) \rightarrow f(x(t), t)\eta(t)$, where f is some function and the random force $\eta(t)$ has a finite correlation time, we can proceed similarly. In this case, the normal distribution of the integrated white noise is replaced with the appropriate distribution of the integrated coloured noise $\int_0^\tau dt' f(x(t'), t')\eta(t') \approx f(x(0), 0) \int_0^\tau dt' \eta(t')$.

After inserting the approximated propagator (14) into the propagator likelihood (4), we perform a one-dimensional maximisation of the propagator likelihood to infer the parameter $\Theta = b/\sigma^2$. In Fig. 4(a) we plot the relative reconstruction errors versus the dimensionless propagation time τ for various sample sizes, both for the approximate short-time propagator and for the exact finite-time propagator, which is known for the OUP. The non-monotonic behaviour of the error for the short-time propagator shows that the optimal choice for τ involves a trade-off between the error made in approximating the propagator (increasing with τ) and the error due to the finite distances between the sampled configurations that are typically crossed in the propagation time, accompanied by numerical instabilities in the exponentially damped tails of the Gaussian propagators (decreasing with τ). Indeed, as the sample size is increased, resulting in lower typical distances between individual samples, both the optimal value of τ and the total reconstruction error decrease. The exact finite-time propagator suffers only from the numerical instabilities in the tails and therefore the error decreases monotonically with τ , converging to the maximum likelihood estimate as expected. Note that the results for the approximate and exact propagators do not converge for $\tau \rightarrow 0$, since the relative difference of the propagators converges to 0 only for the peak $x = y$, even though the absolute difference converges to 0 for all values of x .

Choosing the optimal propagation time. The non-monotonic behaviour of the reconstruction error $\epsilon = |\Theta^{\text{inf}} - \Theta^{\text{true}}|/\Theta^{\text{true}}$ raises the question how to choose the optimal propagation time without prior knowledge of the underlying parameter Θ^{true} . We find an answer by assuming that the error is a smooth function of the propagation time: we seek the minimal error by demanding $0 = \partial\epsilon/\partial\tau = \frac{\text{sgn}(\Theta^{\text{inf}} - \Theta^{\text{true}})}{|\Theta^{\text{true}}|} \frac{\partial\Theta^{\text{inf}}}{\partial\tau} \sim \partial\Theta^{\text{inf}}/\partial\tau$. Realistically, we will not achieve a perfect fit, i.e. $\Theta^{\text{inf}} \neq \Theta^{\text{true}}$ and therefore $\text{sgn}(\Theta^{\text{inf}} - \Theta^{\text{true}}) = \pm 1$. Thus, the error derivative will become small only for $\partial\Theta^{\text{inf}}/\partial\tau \rightarrow 0$. The latter quantity can be estimated directly from the data by repeating the inference for a set of propagation times $\{(\tau_i, \tau_i + \Delta\tau)\}$ and computing the forward difference quotients $\partial\Theta^{\text{inf}}/\partial\tau(\tau_i) \approx [\Theta^{\text{inf}}(\tau_i + \Delta\tau) - \Theta^{\text{inf}}(\tau_i)]/\Delta\tau$. Since estimating the derivative from the data will incur numerical errors, we relax the condition $0 = \partial\Theta^{\text{inf}}/\partial\tau$ and demand only that $|\partial\Theta^{\text{inf}}/\partial\tau|$ is minimal. In Fig. 4(b) we show that these minima indeed coincide with the optimal choice of τ as judged from the reconstruction error shown

in Fig. 4(a).

NON-EQUILIBRIUM MODELS IN STATISTICAL PHYSICS AND THEORETICAL BIOLOGY

We now turn to non-equilibrium applications where the standard maximum likelihood approach is not feasible, as the steady-state distribution is unknown.

The kinetic Ising model

The kinetic Ising model consists of a set of N binary spins $s_i = \pm 1$, which interact with each other via couplings J_{ij} and are subject to external fields h_i (see inset of Fig. 5). Crucially, the couplings are not symmetric ($J_{ij} \neq J_{ji}$ in general). A stochastic dynamics of this model is specified by the so-called Glauber dynamics [11]: In each time step, a spin i is chosen and its value $s_i(t+1)$ one time step later is updated according to the probability distribution

$$p(s_i(t+1)|\mathbf{s}(t)) = \frac{\exp\{s_i(t+1)\theta_i(t)\}}{2 \cosh(\theta_i(t))}, \quad (15)$$

where the effective local field at time t is

$$\theta_i(t) = h_i + \sum_{j=1}^N J_{ij}s_j(t). \quad (16)$$

The kinetic Ising model has been used to model gene regulatory and neural networks [12–14].

For a symmetric coupling matrix without self-couplings, the Glauber dynamics (15) converges to the equilibrium state characterised by the Boltzmann distribution $p_B(\mathbf{s}) = e^{-\mathcal{H}(\mathbf{s})}/Z$ with the well-known Ising Hamiltonian $\mathcal{H}(\mathbf{s}) = -\sum_i s_i(h_i + \sum_{j>i} J_{ij}s_j)$. For asymmetric couplings, however, Glauber dynamics (15) converges to a non-equilibrium steady state, which lacks detailed balance and is hard to characterise.

In recent work we have shown how the spin couplings J_{ij} and external fields h_i can be inferred from independent samples taken from the steady state by fitting couplings and fields to match the magnetisations, two-, and three-point correlations sampled in the data [15]. Here we demonstrate that the couplings can be inferred even more accurately with the propagator likelihood (4), which uses information from the full empirical distribution. We insert the single-step propagator (15) into the propagator likelihood (4) and maximise the propagator likelihood with respect to the external fields h_i and off-diagonal couplings J_{ij} (we consider a model without self-interactions: $J_{ii} = 0$). For the last step, we use the Broyden-Fletcher-Goldfarb-Shanno algorithm as implemented in the SciPy library [10], and initialise the algorithm with the naive mean-field parameter estimates as described in [15]. In

Fig. 5, we compare the relative errors of coupling reconstruction $\epsilon = \|\mathbf{J}^{\text{inf}} - \mathbf{J}^{\text{true}}\|_2 / \|\mathbf{J}^{\text{true}}\|_2$ using the single-step propagator likelihood with those of fitting finite spin moments up to three-point correlations.

It turns out that parameter inference in the kinetic Ising model requires more samples than in the equilibrium inverse Ising problem. To achieve a relative reconstruction error of 10^{-2} for an equilibrium system of $N = 10$ spins, the pseudolikelihood method requires of the order of 10^6 samples [16]. In the non-equilibrium model considered here, we require at least 10^8 samples for a similar reconstruction accuracy (see Fig. 5). The reason for this is that, in the kinetic Ising model, couplings are not uniquely determined by pairwise correlations. Instead, many different models can reproduce the same pairwise correlations. For this reason, we need information from higher order spin correlations, which require more samples to determine them accurately.

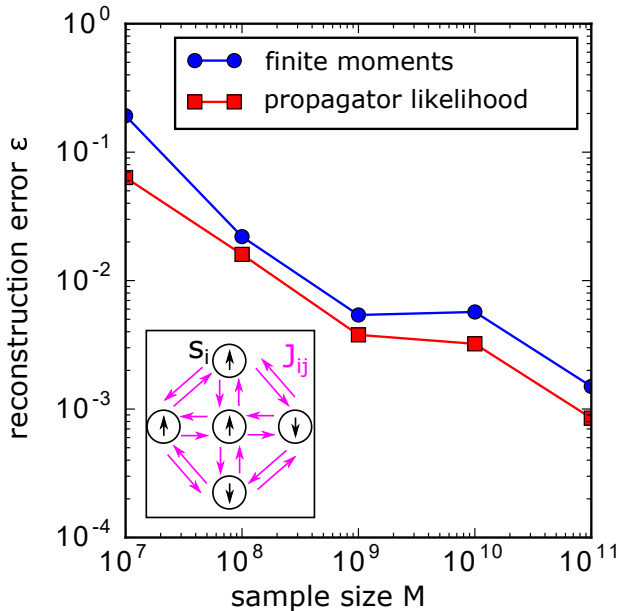


FIG. 5. The inference of couplings in the kinetic Ising model. The inset schematically shows a system of binary spins interacting via couplings J_{ij} subject to external fields h_i (not shown). In the main figure we plot the relative errors of couplings $\epsilon = \|\mathbf{J}^{\text{inf}} - \mathbf{J}^{\text{true}}\|_2 / \|\mathbf{J}^{\text{true}}\|_2$ versus the number of independent samples used for inference, using (i) finite spin moments up to three-point correlations (\bullet) and (ii) the single-step propagator likelihood (\blacksquare). Both methods are exact, so the relative error decreases with the sample size as $\epsilon \sim M^{-1/2}$. The propagator likelihood (which uses the full set of configurations sampled) performs only a little better than the fit to the first three moments, showing that most information required for reconstruction is already contained in the first three moments. The underlying off-diagonal couplings were drawn independently from a Gaussian distribution with mean 0 and standard deviation $1/\sqrt{N}$ (we excluded self-interactions, $J_{ii} = 0$), the external fields were drawn independently from a Gaussian distribution with mean 0 and standard deviation 1. The system size was $N = 10$ spins.

Sparse networks. We consider a particular situation, where the parameter inference requires fewer samples. We consider sparse coupling matrices and assume that the topology of the couplings is known, and only the values of the couplings are needed. Specifically, we consider the kinetic Ising model with sparse couplings (so most interactions are zero) and assume as prior knowledge the pairs (i, j) that have a non-zero coupling between them, i.e. $J_{ij}^{\text{true}} \neq 0$ or $J_{ji}^{\text{true}} \neq 0$, regardless of the direction of the coupling. The problem has been addressed for undirected equilibrium systems like Ising models with ferromagnetic or binary couplings [16, 17]. We apply the propagator likelihood to a network of $N = 10$ spins, where each possible directed link J_{ij} from spin i to spin j is non-zero with probability $p = 0.2$. The non-zero couplings are again drawn independently from a Gaussian distribution with mean 0 and variance $1/N$. Self-interactions are excluded and the external fields h_i drawn independently from a Gaussian distribution with mean 0 and variance 1. Figure 6 shows that the directed couplings can be inferred with slightly fewer samples when the topology of the couplings is known.

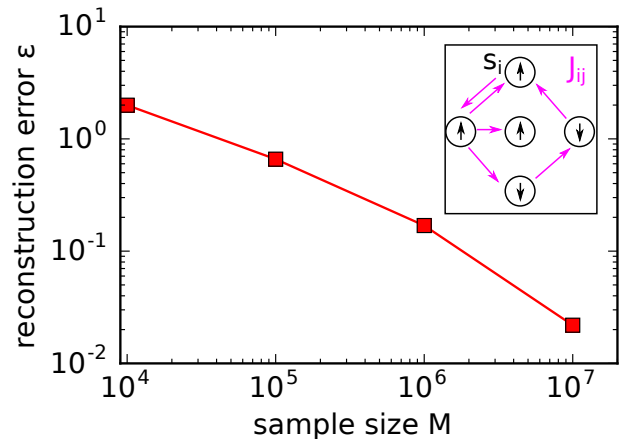


FIG. 6. Coupling inference in the sparse kinetic Ising model. The inset schematically shows a system of binary spins interacting via sparse couplings J_{ij} subject to external fields h_i (not shown). In the main figure, we plot the relative errors of couplings $\epsilon = \|\mathbf{J}^{\text{inf}} - \mathbf{J}^{\text{true}}\|_2 / \|\mathbf{J}^{\text{true}}\|_2$ versus the number of independent samples. The underlying off-diagonal couplings were chosen sparsely: they were set to zero with probability $1 - p = 0.8$, and with probability $p = 0.2$ were drawn independently from a Gaussian distribution with mean 0 and variance $1/N$ (we excluded self-interactions, $J_{ii} = 0$). The external fields were drawn independently from a Gaussian distribution with mean 0 and variance 1. The system size was $N = 10$ spins. The couplings were inferred by maximising the single-step propagator likelihood over the set of couplings between directly interacting spin pairs (i, j) , i.e. there is at least one true non-zero coupling between the spin pair, $J_{ij}^{\text{true}} \neq 0$ or $J_{ji}^{\text{true}} \neq 0$, regardless of the direction.

Increasing the propagation time. So far we have restricted ourselves to the single-step propagator ($\tau = 1$).

Next, we address the question whether the inference can be improved by increasing the propagation time. Intuitively, we expect that the single-step propagator is optimal when all configurations have been sampled, since this implies that all transitions over longer propagation times consist of single-step transitions that have already been probed by the single-step propagator likelihood: $x^\nu \xrightarrow{\tau} x^\mu = \sum_{x_1, x_2, \dots, x_{\tau-1}} x^\nu \xrightarrow{\tau-1} x_1 \xrightarrow{\tau-1} x_2 \dots \xrightarrow{\tau-1} x_{\tau-1} \xrightarrow{\tau-1} x^\mu$. Indeed, the examples with discrete time considered so far in this article fall into this category and our numerical evidence confirms that increasing the propagation time does not improve the inference. If, however, the configuration space is undersampled, some of the trajectories considered by the longer-time propagator will involve intermediate configurations that are not present in the sample and are therefore not considered by the single-step propagator. In this case, we find that increasing the propagation time does improve the inference for a fixed sample size. In Fig. 7 we consider a kinetic Ising model where only a small fraction of system configurations is present in the sample. Increasing the propagation time from $\tau = 1$ to $\tau = 3$ improves the inference markedly, however, the reconstruction error is considerably smaller for the symmetric part of the coupling matrix [shown in Fig. 7(a)] than for the antisymmetric part [shown in Fig. 7(b)]. This is because the symmetric part of the couplings is governed by the pairwise spin-correlations, while the antisymmetric part is dominated by higher-order spin-correlations, which require more samples for an accurate computation (see [15]). The benefit of increasing the propagation time is also larger for the symmetric part, suggesting that the reconstruction of the antisymmetric part of the couplings is mainly limited by the sample size and that increasing the propagation time even further will not lead to an accurate reconstruction.

The replicator model

The replicator model describes the dynamics of self-replicating entities, for instance genotypes, different animal species, RNA-molecules, or an abstract strategy in the game-theoretic problem. The replicator model has been used in population genetics, ecology, prebiotic chemistry, and sociobiology [18]. We consider a population consisting of N different species and denote by x_i the fraction of species i in the total population (scaled for convenience by a factor on N so $\sum_i x_i = N$). The growth rate of species i , called its fitness, is denoted by f_i . The population fraction change in time depends on the growth rate f_i and the average growth rate of the population \bar{f}

$$\frac{dx_i}{dt} = x_i(t)(f_i(\mathbf{x}, t) - \bar{f}(\mathbf{x}, t)), \quad (17)$$

with $\bar{f}(\mathbf{x}, t) = \frac{1}{N} \sum_{j=1}^N x_j(t) f_j(\mathbf{x}, t)$. The set of equations (17) defines the replicator model. The average fitness \bar{f} enters to ensure that the fractions remain normalised such that $\sum_i x_i(t) = N$ for all times.

Here we consider a fitness which for each species i depends linearly on the population fractions of the other species

$$f_i(\mathbf{x}(t)) = \sum_{j \neq i}^N J_{ij} x_j(t). \quad (18)$$

The inter-species interactions J_{ij} are quenched random variables with mean u (corresponding to a cooperation pressure) and standard deviation $1/\sqrt{N}$. There are no self-interactions, i.e. $J_{ii} = 0$.

For symmetric interactions, $J_{ij} = J_{ji}$, the fitness vector can be written as the gradient of a Lyapunov function. This implies that the system converges to an equilibrium steady state, which can be characterised by methods from statistical physics [19]. In the socio-biological context, however, there is no reason for the interactions to be symmetric, or in fact to assume deterministic dynamics. Assuming an asymmetric matrix J_{ij} and allowing random fluctuations $\sigma \xi_i(t)$ in the reproduction of species i leads to a set of Langevin equations

$$\frac{dx_i}{dt} = x_i(t) (f_i(\mathbf{x}(t)) + \sigma \xi_i(t) - \lambda(\mathbf{x}, t)), \quad (19)$$

where the $\xi_i(t)$ are N independent sources of white noise interpreted in the Stratonovich convention, the parameter $\sigma > 0$ controls the overall noise strength, and the factor $\lambda(\mathbf{x}(t), t) = \frac{1}{N} \sum_j x_j(t) (f_j(\mathbf{x}(t)) + \sigma \xi_j(t))$ ensures normalisation, i.e. $\sum_i x_i(t) = N$ for all times. This dynamics converges to a non-equilibrium steady state. Its characteristics for typical realisations of the matrix of couplings have been studied in the limit of a large number of species using dynamical mean field theory [20].

We now turn to the problem of inferring the couplings J_{ij} of the replicator model from a set of configurations $\{\mathbf{x}^\mu\}_{\mu=1}^M$ taken independently from the non-equilibrium steady state. For simplicity, we focus on the so-called cooperative regime, in which all species survive in the long-time limit, i.e. $\lim_{t \rightarrow \infty} x_i(t) > 0 \forall i$. This regime is characterised by a sufficiently large value of the cooperation pressure u [20]. Our results can be generalised to the case where species go extinct by restricting the transitions $\mathbf{x}^\nu \rightarrow \mathbf{x}^\mu$ considered in the propagator likelihood to those between configurations with the same set of surviving species.

Again, to make time dimensionless, we rescale time $t' = t\sigma^2$, resulting in a noise-term with unit magnitude. The steady state and the propagator depend only on the rescaled couplings $\hat{J}_{ij} \equiv J_{ij}/\sigma^2$. By linearising the LE (19) for short times and eliminating x_N via the normalisation constraint, $x_N = N - \sum_{i=1}^{N-1} x_i$, we arrive at

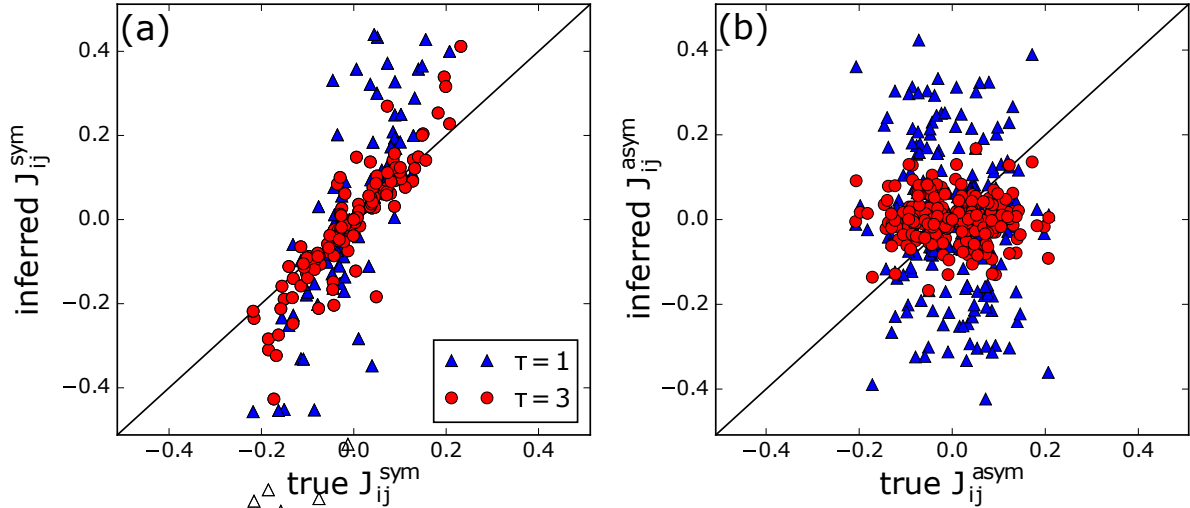


FIG. 7. Increasing the propagation time in the undersampled kinetic Ising model. (a) shows the reconstructed symmetric part of the coupling matrix $J_{ij}^{\text{sym}} = (J_{ij} + J_{ji})/2$ for inference with the single-step propagator likelihood (\blacktriangle) and for inference with the longer propagation time $\tau = 3$ (\bullet). (b) shows the reconstructed antisymmetric part of the coupling matrix $J_{ij}^{\text{asym}} = (J_{ij} - J_{ji})/2$ for inference with the single-step propagator likelihood (\blacktriangle) and for inference with the longer propagation time $\tau = 3$ (\bullet). The underlying off-diagonal couplings were drawn independently from a Gaussian distribution with mean 0 and standard deviation $0.5/\sqrt{N}$ (we excluded self-interactions, $J_{ii} = 0$), the external fields were drawn independently from a Gaussian distribution with mean 0 and standard deviation 0.5. The system size was $N = 16$ spins and $M = 10^4 N$ samples were used. As a result, less than a third of the 2^{16} system configurations were present in the sample.

an approximate Gaussian propagator

$$p(\mathbf{x}, \tau | \mathbf{y}, 0) \approx \frac{1}{\sqrt{2\pi\tau}^{N-1} \sqrt{\text{Det}\Sigma}} \times \exp \left\{ -\frac{1}{2\tau} \sum_{i,j=1}^{N-1} (x_i - y_i - \mu_i\tau) \Sigma_{ij}^{-1} (x_j - y_j - \mu_j\tau) \right\} \quad (20)$$

with drift ¹

$$\mu_i = y_i(\hat{f}_i(\mathbf{y}) - \bar{f}(\mathbf{y})) - \frac{y_i}{N} \left(y_i - \frac{1}{N} \sum_{j=1}^N y_j^2 \right) \quad (21)$$

and covariance matrix $\Sigma = AA^T \in \mathbb{R}^{N-1 \times N-1}$ with

$$A_{ij} = y_i(y_j/N - \delta_{i,j}). \quad (22)$$

We denote by $\hat{f}_i(\mathbf{y})$ the fitness (18) calculated with the rescaled variables $\hat{J}_{ij} = J_{ij}/\sigma^2$, instead of the original interactions J_{ij} , and by $\bar{f}(\mathbf{y}) = \frac{1}{N} \sum_j y_j \hat{f}_j(\mathbf{y})$ its species-weighted average.

¹ The second term in the drift arises from the difference between the Itô and Stratonovich convention in the Langevin equation.

To reconstruct the rescaled interactions \hat{J}_{ij} , we insert the approximate propagator (20) into the propagator likelihood (4) and maximise it using the Broyden-Fletcher-Goldfarb-Shanno algorithm (see Fig. 8). As for the OUP, the reconstruction error depends non-monotonically on the choice of the dimensionless propagation time τ , due to the tradeoff between the error from linearising the LE and the error from the numerical evaluation of the exponentially damped propagators. Unfortunately, the simple procedure we used for the OUP, i.e. minimising the parameter derivative $|\partial\Theta^{\text{inf}}/\partial\tau|$, cannot easily be generalised to higher dimensions. The reason is that the derivative of the reconstruction error $\partial\epsilon/\partial\tau$ is a linear combination of the individual parameter entries $(\partial\Theta_i^{\text{inf}}/\partial\tau)_{i=1}^K$, which can cancel each other without vanishing individually (here $K = N(N-1)$ denotes the number of model parameters). To see that not all individual derivatives can vanish simultaneously, we remind ourselves that the inferred parameters must satisfy $0 \equiv \frac{\partial\mathcal{P}\mathcal{L}}{\partial\Theta_i}(\Theta^{\text{inf}}(\tau), \tau)$, $i = 1, \dots, K$. Additionally demanding $\partial\Theta_i^{\text{inf}}/\partial\tau = 0$, $i = 1, \dots, K$, corresponds to solving the system of equations $\{\frac{\partial\mathcal{P}\mathcal{L}}{\partial\Theta_i} = 0, \frac{\partial^2\mathcal{P}\mathcal{L}}{\partial\Theta_i\partial\tau} = 0\}_{i=1}^K$ for the $K+1$ variables (Θ_i, τ) . This system of $2K$ nonlinear equations for $K+1$ variables will in general have no solution for $K > 1$. Instead, we can find a good propagation time by plotting a single inferred parameter versus the propagation time τ used for inference [see Fig. 8(b)]. The regime where the inference is dominated

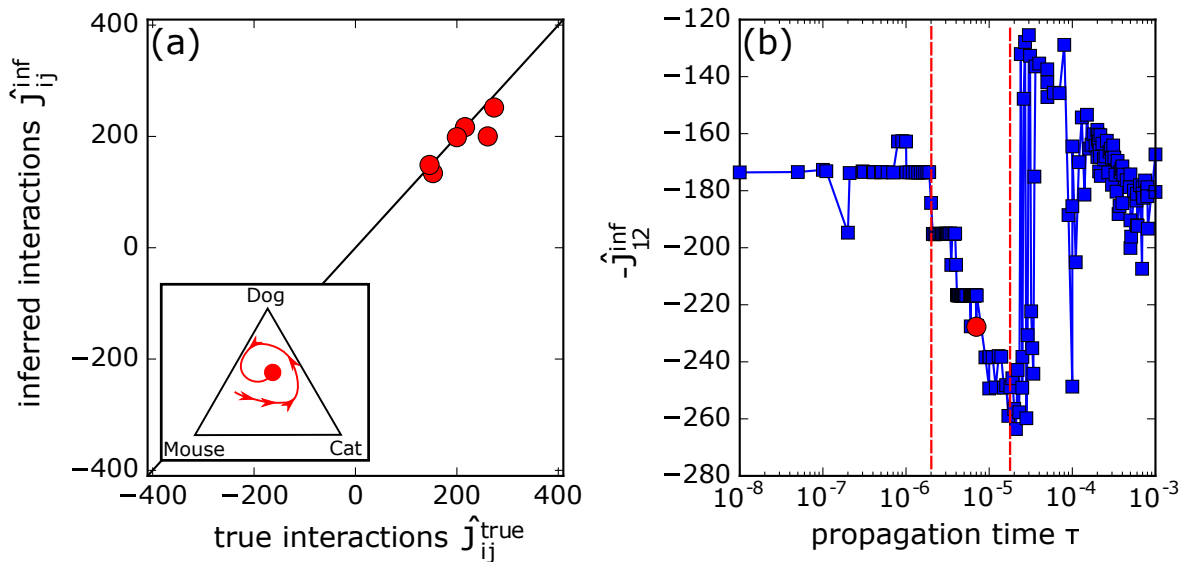


FIG. 8. Reconstruction of the inter-species interactions in replicator dynamics.

(a) The inset schematically shows the dynamical model of different species competing for fractions of the total population size. The population moves on a N -dimensional simplex defined by the normalisation $\sum_i x_i = N$, $x_i \geq 0$. In the main figure, we plot the inferred rescaled inter-species interactions $\hat{J}_{ij}^{\text{inf}} \equiv J_{ij}^{\text{inf}}/\sigma^2$ versus the rescaled underlying interactions $\hat{J}_{ij}^{\text{true}} = J_{ij}^{\text{true}}/\sigma^2$ for the propagation time $\tau = 5.0 \times 10^{-6}$. (b) shows how the propagation time was chosen. An arbitrary parameter (here \hat{J}_{12}) is chosen and its inferred value plotted for several different propagation times τ_i . For large τ , the error in the linearisation of the Langevin equations becomes large and the inference becomes unstable, as signalled by the erratic changes in the value of the inferred parameter. For small values of τ , most transition probabilities are damped exponentially and the numerical inaccuracies in the evaluation of these exponentials results in a saturation of the parameter value. Reasonable propagation times must lie between those two regimes and we choose a propagation time (marked by the red circle) that lies in the centre of this transition region (marked by the dashed lines). The other parameters (not shown) show a similar behaviour with the same transition region.

The system consisted of $N = 3$ species, the noise strength was set to $\sigma = 0.1$, and the underlying interactions J_{ij}^{true} were quenched random variables chosen independently from a Gaussian with mean $u = 2.0$ and standard deviation $1/\sqrt{N}$ (no self-interactions: $J_{ii} = 0$). We used an Euler discretisation of the Langevin equation (19) with time steps of length $\Delta t = 10^{-6}/\sigma^2$ and a total of $M = 10^3$ samples were taken every 10^4 steps after an initial settling time of 10^9 steps.

by the error from the linearisation for large values of τ is characterised by an erratic change of the value of the inferred parameter. The regime dominated by the error from the exponential damping for small values of τ is characterised by a saturation of the inferred parameter. These regimes are connected by a transition region, from which the propagation time should be chosen. Here, we choose a propagation time that lies in the centre of this transition region and find this produces a good (although not necessarily optimal) reconstruction quality.

CONCLUSIONS

We developed a method to infer the parameters of a Markov process from independent samples taken from the steady state and applied it to different non-equilibrium models. The method is based on an extension of the principle of maximum likelihood: our propagator likelihood finds model parameters for which the distribution of

configurations sampled from the steady state is invariant under propagation in time. For systems with discrete time, we found that the single-step propagator is sufficient, although increasing the propagation time improves the inference when not all configurations have been sampled. For systems with continuous time, we showed that there is an optimal propagation time, balancing the error from linearising the Langevin equation (increasing with τ) and the numerical error from evaluating exponentially damped propagators (decreasing with τ). For the Ornstein-Uhlenbeck process, we chose the optimal propagation by demanding that the inferred parameter becomes stationary with respect to the propagation time $\partial\Theta^{\text{inf}}/\partial\tau \stackrel{!}{=} 0$, for higher-dimensional systems like replicator dynamics, we could only identify a region of suitable propagation times without a recipe for determining which propagation time is optimal.

Inferring model parameters from the steady state requires a large number of samples. It is also computationally expensive: evaluating the propagator likelihood requires

$\mathcal{O}(M^2)$ operations for systems with continuous configurations and $\mathcal{O}(M)$ operations for systems with discrete configurations, provided there are only a small number of neighbouring configurations that can be reached in a single step with non-zero transition probability. In the future it would be interesting to find approximations that allow for a more efficient computation of the propagator likelihood, thus making parameter inference feasible for larger systems.

* sdettmer@thp.uni-koeln.de, and berg@thp.uni-koeln.de

- [1] H. C. Nguyen, R. Zecchina, and J. Berg, arXiv preprint [arXiv:1702.01522](https://arxiv.org/abs/1702.01522), to appear in *Advances in Physics* (2017).
- [2] Y. Roudi and J. Hertz, *Phys. Rev. Lett.* **106**, 048702 (2011).
- [3] H.-L. Zeng, M. Alava, E. Aurell, J. Hertz, and Y. Roudi, *Phys. Rev. Lett.* **110**, 210601 (2013).
- [4] M. Mézard and J. Sakellariou, *J. Stat. Mech.*, L07001 (2011).
- [5] H. Mahmoudi and D. Saad, *J. Stat. Mech.*, P07001 (2014).
- [6] S. Kullback and R. A. Leibler, *Ann. Math. Statist.* **22**, 79 (1951).
- [7] J. Krug and P. Ferrari, *J. Phys. A-Math. Gen.* **29**, L465 (1996).
- [8] M. Evans, *J. Phys. A-Math. Gen.* **30**, 5669 (1997).
- [9] B. Derrida, *Phys. Rep.* **301**, 65 (1998).
- [10] E. Jones, T. Oliphant, P. Peterson, *et al.*, “SciPy: Open source scientific tools for Python,” (2001–), [Online; accessed 2016-07-08].
- [11] R. J. Glauber, *J. Math. Phys.* **4**, 294 (1963).
- [12] B. Derrida, E. Gardner, and A. Zippelius, *Europhys. Lett.* **4**, 167 (1987).
- [13] J. Hertz, A. Krogh, and R. G. Palmer, *Introduction to the theory of neural computation*, Vol. 1 (Addison-Wesley Publishing Company, 1991).
- [14] M. Bailly-Bechet, A. Braunstein, A. Pagnani, M. Weigt, and R. Zecchina, *BMC Bioinformatics* **11**, 355 (2010).
- [15] S. L. Dettmer, H. C. Nguyen, and J. Berg, *Phys. Rev. E* **94**, 052116 (2016).
- [16] E. Aurell and M. Ekeberg, *Phys. Rev. Lett.* **108**, 090201 (2012).
- [17] J. Bento and A. Montanari, *Adv. Neural Inf. Process. Syst.* **22** (2009).
- [18] P. Schuster and K. Sigmund, *J. Theor. Biol.* **100**, 533 (1983).
- [19] S. Diederich and M. Oppen, *Phys. Rev. A* **39**, 4333 (1989).
- [20] M. Oppen and S. Diederich, *Phys. Rev. Lett.* **69**, 1616 (1992).